Interactions of Deglycosylated Cobalt(III)−Pepleomycin (Green Form) with DNA Based on NMR Structural Studies[†,⊥]

Janet Caceres-Cortes,[‡] Hiroshi Sugiyama,[§,||] Kenji Ikudome,[§] Isao Saito,[§] and Andrew H.-J. Wang*,[‡]

Department of Cell and Structural Biology, University of Illinois at Urbana−Champaign, Urbana, Illinois 61801, and Department of Synthetic Chemistry and Biological Chemistry, Faculty of Engineering, Kyoto University, Kyoto 606-01, Japan

Received April 17, 1997; Revised Manuscript Received June 11, 1997[⊗]

ABSTRACT: Pepleomycin (PEP)[1] is a metalloglycopeptide antitumor antibiotic that has improved pharmacological properties than does bleomycin (BLM). Both PEP and BLM bind to and degrade DNA in a sequence-selective manner. The binding interactions of HO_2^-−Co(III)−CodPEP (CodPEP) with CGTACG have been studied by 2D NMR and molecular modeling. Inspection of the 2D-NMR data revealed 60 notable intermolecular NOEs between CodPEP and CGTACG which place the drug's metal binding domain and peptide linker in the minor groove of the DNA close to G8 and T9. On the basis of the NOEs, the drug's DNA binding domain is located close to the T9·A4 and A10·T3 base pairs. Intercalation of the bithiazole tail between these base pairs is indicated by the loss of DNA symmetry upon complexation with CodPEP, by a break in the sequential connectivity at the TpA steps, and by the upfield shift of the bithiazole H-H5 and H-H5′ proton resonances. Intercalation of the bithiazole moiety unfolds the CodPEP molecule and exposes its hydroperoxide group to the DNA. The hydroperoxide group in the refined model of CodPEP−CGTACG is close to the C4′ proton of T9, consistent with cleavage at this position. The NOE pattern between the pyrimidine ring of CodPEP and G8 of DNA suggests a specific pairing recognition via hydrogen bonds between these groups, thus establishing a 5′-GT-3′ sequence preference. The structural elucidation of the free CodPEP and CoPEP [Caceres-Cortes et al. (1997) *Eur. J. Biochem. 244*, 818−828], and of the complex of CodPEP-CGTACG afford a plausible mechanism for the recognition and its subsequent cleaving of DNA by the drug. The process involves the unfolding of the compact CodPEP, recognition of a guanine base using the metal binding domain, threading of the bithiazole tail between base pairs, and finally positioning of the HO_2^- group close to the T or C found 3′ to the specific G site.

The metalloglycopeptide antitumor antibiotic pepleomycin (PEP)[1] is more effective in the treatment of certain cancers and has less pulmonary toxicity than bleomycin (BLM) (Oka, 1980; Takahashi et al., 1979; Matsuda et al., 1978). The structures of PEP and BLM are similar (Figure 1). They each contain nine fragments that are commonly divided into a metal binding domain (A, P, and H moieties), a DNA binding domain (B and S groups), a peptide linker (V and T fragments), and a disaccharide moiety (G and M groups). BLMs and PEP differ only in the C-terminal substituent. BLM A_2 and BLM B_2 contain a terminal cationic functional group at the C-terminus, while PEP contains a neutral phenyl group at this position.

PEP, like BLM, exerts its action by binding to and degrading DNA in a sequence-selective manner (D'Andrea & Haseltine, 1978; Takita et al., 1978). DNA degradation by PEP requires prior activation of the drug with molecular oxygen and certain metals such as Fe(II) and Co(III) (Xu et al., 1992a,b; Burger et al., 1980). Once activated, PEP initiates DNA damage by abstracting the hydrogen atom at the C4′ position of deoxyribose (Wu et al., 1985; McGall et al., 1987). The resulting free radical containing DNA intermediate is unstable and undergoes further degradation by two pathways. Under anaerobic conditions, degradation results in the liberation of free nucleic acid bases and the formation of an oxidatively damaged sugar that cleaves upon treatment with hydroxide ion (Burger et al., 1982). In the presence of oxygen, degradation results in the cleavage of the deoxyribose C3′−C4′ bond with the release of a base propenal, a 5′-phosphate ester, and a 3′-phosphoglycolate group (Burger et al., 1981). DNA degradation by these pathways is sequence dependent, producing single strand

[†] This work was supported by a grant from the American Cancer Society (DHP-114A) to A.H.-J.W. The Kyoto part of this work was supported by a Grant-in Aid for Scientific Research from the Ministry of Education, Science and Culture, Japan, and by CREST (Core Research for Evolutional Science and Technology) of Japan Science and Technology Corp. (JST). Support to J.C.-C. by an NIH Radiation, Biophysics and Bioengineering in Oncology Traineeship (PHS 5 T32 CA09067) is acknowledged. The Varian VXR500 NMR spectrometer at UIUC was supported in part from NIH Shared Instrumentation Grant 1S10RR06243.

[⊥] Coordinates have been deposited in the Brookhaven Protein Data Bank under the accession numbers 1ao1, 1ao2, and 1ao4 for CodPEP−CGTACG, CodPEP, and CoPEP, respectively.

* To whom correspondence should be addressed.

[‡] University of Illinois.

[§] Kyoto University.

[||] Present address: Institute for Medical and Dental Engineering, Tokyo Medical and Dental University, 2-3-10 Kanda Surugadai Chiyoda-Ku, Tokyo 101, Japan.

[⊗] Abstract published in *Advance ACS Abstracts,* August 1, 1997.

[1] Abbreviations: PEP, pepleomycin or N^1-[3-[[(*S*)-α-methylbenzyl]-amino]propyl]bleomycinamide; BLM, bleomycin; bleomycin A_2, N^1-[3-(dimethylsulfonio)propyl]bleomycinamide; CoPEP, HO_2^-−Co(III)−pepleomycin; CodPEP, deglycosylated CoPEP or deglycosylated HO_2^-−Co(III)−pepleomycin which lacks the sugars gulose and mannose; A-NH_2, β-aminoalanine amine group; M-NH_2, mannose carbamoyl group; 1D and 2D, one and two dimensional; NMR, nuclear magnetic resonance; UV, ultraviolet; NOE, nuclear Overhauser effect; NOESY, NOE spectroscopy; TOCSY, total correlation spectroscopy; T_1IR, T_1 relaxation inversion recovery; DSS, 2,2-dimethyl-2-silapentene-5-sulfonate; ppm, parts per million; SPEDREF, spectral-driven refinement.

S0006-2960(97)00895-7 CCC: $14.00

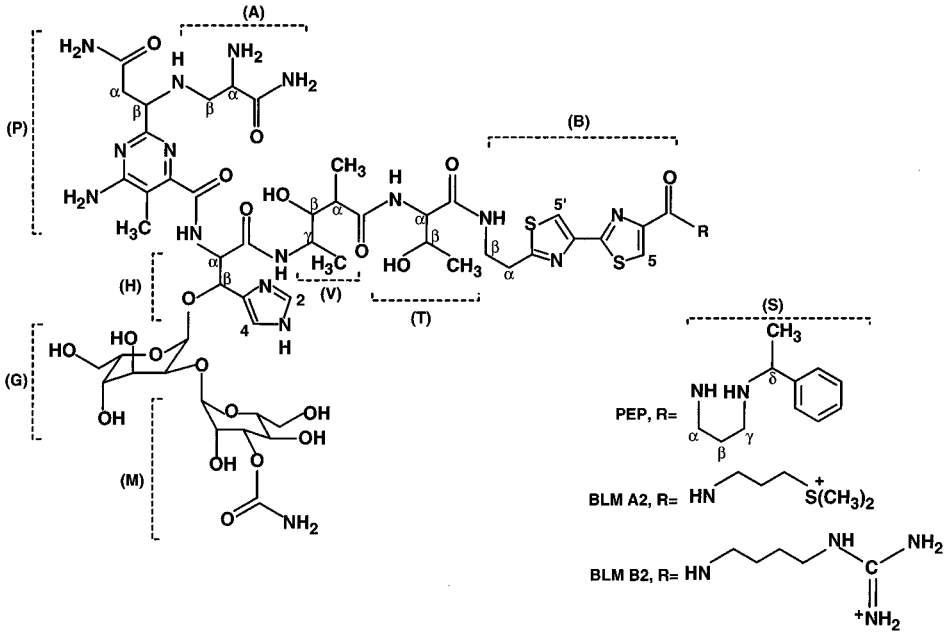

FIGURE 1: Molecular structure of pepleomycin (PEP) and two bleomycin (BLM) drugs. Each structure consists of nine fragments identified with dotted lines and abbreviated as follows: (A) β-aminoalanine, (P) pyrimidinyl propionamide, (H) β-hydrohistidine, (V) methyl valerate, (T) threonine, (B) bithiazole, (G) α-L-gulose, (M) α-D-mannose, and (S) the C-terminal substituent. PEP and BLMs differ in the C-terminal substituent. These substituents are 3-[(*S*)-(1-phenylethyl)amino]propylamine for PEP and γ-aminopropyldimethylsulfonium for BLM A_2.

scissions at 5′-GC-3′ and 5′-GT-3′ sequences (D'Andrea & Haseltine, 1978; Takeshita et al., 1978; Mirabelli et al., 1983). Despite the intense investigations in this area, the basis for this sequence specificity is still not clear. This is due, in part, to the continuing uncertainty concerning the exact metal ligands of these drugs and their mode of binding to DNA.

We have recently defined the axial ligands and the chirality around the metal center of two cobalt−pepleomycin species, HO_2^-−Co(III)−PEP (CoPEP) and deglycosylated HO_2^-−Co(III)−PEP (CodPEP) (Caceres-Cortes et al., 1997). Earlier studies of the related HO_2^--Co(III)-BLM A_2 proposed that the β-aminoalanine amine (A-NH_2) group was the preferred axial ligand (Xu et al., 1994; Wu et al., 1996a). These studies, however, were limited by the incomplete resonance assignment of the exchangeable protons. Our complete resonance assignments and detailed spectral analysis of CoPEP and CodPEP revealed that A-NH_2 is not the preferred axial ligand in CoPEP. Instead, the mannose carbamoyl (M-NH_2) group is the preferred axial ligand in metal complexes containing an intact PEP or BLM molecule (Figure 2B). When the drugs do not contain the disaccharide moiety, as in the deglycosylated CodPEP species, A-NH_2 comes to occupy the axial position, thus maintaining a square bipyramidal geometry around the cobalt (Figure 2A). These results are consistent with those obtained for CO−Fe(II)−BLM A_2 in which the mannose M-NH_2 group is ligated to iron (Akkerman et al., 1990) and with the studies performed on a fragment of Co(III)−BLM A_2 lacking the disaccharide and DNA binding part, in which A-NH_2 is the axial ligand (Dabrowiak & Tsukayama, 1981).

DNA binding by PEP and BLM involves the metal (Shipley & Hecht, 1988; Sugiyama et al., 1986; Carter et al., 1990) and the DNA binding domains (Chien et al., 1977; Povirk et al., 1979; Kross et al., 1982; Fisher et al., 1985). The metal binding domain interacts with the minor groove of the DNA and is believed to confer the sequence selectivity of the drug (Sugiyama et al., 1986; Kane et al., 1994; Wu et al., 1985; Kozarich et al., 1989). The DNA binding domain can interact with the minor groove or intercalate between the DNA base pairs (Hiraoki et al., 1991; Povirk et al., 1979; Chen et al., 1980; Hénichart et al., 1985; Kuwahara et al., 1988), thus helping to stabilize the drug−DNA complex. Interestingly, differences in the metal binding domains of various BLMs appear to affect the interactions of these drugs with DNA. Treatment of d($CGCT_3A_3GCG)_2$ with Fe−BLM, deglycosylated Fe−BLM, and decarbamoyl Fe−BLM results in preferential cleavage at different sites (Sugiyama et al., 1986). Cleavage with Fe−BLM occurs predominantly at C11 while cleavage with deglycosylated Fe−BLM and

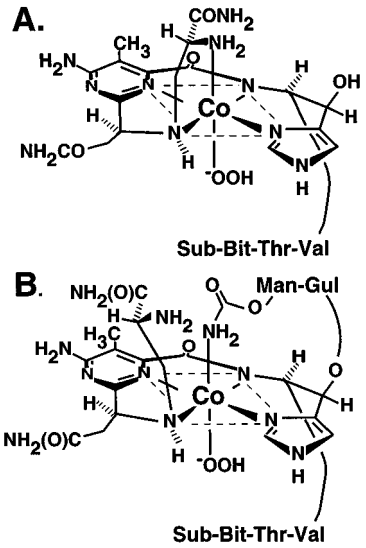

FIGURE 2: Schematic representations of CodPEP and CoPEP showing the orientation of PEP ligands around cobalt(III). Five nitrogen donor atoms from PEP and a hydroperoxide group bind to cobalt in a square bipyramidal geometry. The equatorial ligands include the secondary amine of A, the pyrimidine N5 of P, and the imidazole N1 and the amide nitrogens of H. The axial ligands are A-NH_2 and HO_2^- for CodPEP (A) and M-NH_2 and HO_2^- for CoPEP (B).

decarbamoyl Fe−BLM occurs predominantly at C3. It is still not clear whether the different interactions between DNA with Fe−BLM and deglycosylated Fe−BLM are due to the nature of the axial ligands (M-NH_2 or A-NH_2), arise because of added steric effects from the presence of the sugars, or are a result of the combination of both of these factors. The possibility that the different sequence contexts around C3 and C11 is also influencing drug binding to DNA cannot be excluded.

At present, there is no consensus regarding the binding mode(s) of the C-terminus of BLM to DNA or the role of the DNA sequence context in defining the binding mode(s) of this group. NMR studies of the interaction of Zn(II)−BLM A_5 with $d(CGCTAGCG)_2$ have indicated multiple binding modes of the C-terminus, including one that involves binding of the bithiazole within the minor groove of the DNA (Manderville et al., 1994, 1995). More recent studies of Co(III)−BLM A_2 binding to $d(CCAGGCCTGG)_2$ established that the mode of binding of the C-terminus involves intercalation (Wu et al., 1994, 1996a,b).

In an effort to characterize the mode of binding of CoPEP and CodPEP to DNA and reveal any structural variations that may arise in the drug−DNA complexes as a result of the differences in the metal binding domains of CoPEP and CodPEP, we have investigated the interactions between these drugs and various oligodeoxynucleotides. In the present paper, we report the structural details of the complex formed between CodPEP and the self-complementary hexamer CGTACG.

MATERIALS AND METHODS

Sample Preparation. (A) CodPEP and DNA. A lyophilized sample of HPLC-purified HO_2^-−Co(III)−CodPEP (CodPEP) (green form) was prepared as described previously (Sugiyama et al., 1990; Boger et al., 1992). An NMR solution was prepared by dissolving the appropriate amounts of CodPEP in 500 μL phosphate buffer solution (50 mM sodium phosphate, pH 6.4, and 0.15 M NaCl). The solution was lyophilized three times with 99.8% D_2O, then redissolved in 250 μL of 99.96% D_2O, and transferred to an NMR tube. The solution was then dried with a stream of nitrogen gas and redissolved in 500 μL of 99.96% D_2O. The final drug concentration was 2.41 mM.

The oligonucleotide CGTACG was synthesized on a DNA synthesizer in the Genetic Facility at University of Illinois. The sample was purified by Sepharose G-50 column chromatography and lyophilized. An NMR sample of CGTACG (3.0 mM) was prepared by dissolving the DNA in 500 μL phosphate buffer (50 mM sodium phosphate, pH 7.0, and 0.15 M NaCl). The sample was then lyophilized as described above.

(B) CodPEP−CGTACG. Solutions of CodPEP−CGTACG (1 and 2 mM) for NMR studies were prepared by dissolving the DNA oligomer plus appropriate amounts of CodPEP stock solution in 500 μL sodium phosphate buffer (10 and 20 mM, respectively, pH 6.9) The solutions were combined, and the resulting 3 mM solution of CodPEP−CGTACG was desalted using a prepacked NAP-5 column (Pharmacia). The sample was lyophilized three times with 99.8% D_2O, then redissolved in 250 μL of 99.96% D_2O, and transferred to an NMR tube. It was then dried with a stream of nitrogen gas and redissolved in 500 μL of 99.96% D_2O.

A second 1:1 CodPEP−CGTACG sample (4.34 mM) was prepared as described above. The 1:1 drug:DNA sample was titrated with excess CodPEP to reach a 2:1 drug:DNA ratio. CodPEP was added in 0.10 mM increments until a 1.6:1 drug:DNA ratio was reached. CodPEP was then titrated in 0.20 mM increments to reach a final 2:1 drug:DNA ratio. The stepwise addition of CodPEP was monitored by 1D ^1H NMR.

DNA Cleavage of CGTACG by CodPEP. The reaction mixtures (total volume 50 μL) contained 83 μM (duplex concentration) hexamer, 50 mM sodium cacodylate (pH 7.0), and 83 μM green CodPEP. After irradiation (transilluminator TL 33, 366 nm) for 3 h at 0 °C from the distance of 10 cm, 10 μL of the aliquot was taken up and subjected to HPLC analysis. The structures of a 4′-hydroxylated abasic site-containing oligomer was confirmed by hydrazine treatment as described previously (Boger et al., 1992).

NMR Data Collection. NMR measurements were made on a Varian VXR500 spectrometer or an Unity 750 spectrometer. One-dimensional ^1H NMR spectra were recorded for all drug, DNA, and drug−DNA samples at 2 °C unless otherwise stated. The chemical shifts in parts per million (ppm) were referenced to the HDO peak, which is calibrated to 2,2-dimethyl-2-silapentene-5-sulfonate (DSS) at different temperatures. The T_1 relaxation experiment (T_1IR) for CodPEP−CGTACG was carried out with the standard 180°−τ−90° inversion recovery sequence.

Phase-sensitive NOESY spectra with mixing times of 200 ms were recorded for CodPEP−CGTACG using the TPPI−States techniques (States et al., 1982) for phase cycling. The data sets consisted of 2048 complex points in the t_2 dimension and 512 complex free induction decays (FIDs) in the t_1 dimension with 16 transients per FID. The recycle delay was 2.73 s. The 2D data sets were processed with the program FELIX (Hare Research, Woodinville, WA) using Silicon Graphics workstations. In both t_1 and t_2 time domains, the NOE data were apodized to reduce truncation effects by having the last quarter of the FID smoothly attenuate to zero with a sine-bell-squared curve. The resulting FID was exponentially multiplied with a constant of 6 Hz. The data set was then zero-filled in t_1 to 2048 points prior to transformation.

A TOCSY spectrum was obtained for CodPEP−CGTACG with 2048 points in the t_2 dimension and 512 complex FIDs in the t_1 dimension with eight transients per FID. Both time domain data sets were multiplied by a sine-bell-squared window function.

2D-NOESY spectra of the exchangeable protons were collected in 90% H_2O/10% D_2O at 2 °C. The experiments were performed using the 1:1 pulse sequence (Hore, 1983) as the read sequence to give on-resonance suppression of the solvent peak. Radiation damping was avoided using the method described by Sklenar et al. (1987). The offset was set to one-quarter the sweep width to get maximum excitation. The 2D spectra were recorded as 512 t_1 increments of 2048 complex points in t_2 over a sweep width of 12000 Hz and averaged over 32 transients per FID with a mixing time of 80 ms.

Structural Refinement. A previously refined model of CodPEP (Caceres-Cortes et al., 1997) with the β-aminoalanine primary amine as the axial ligand was used to construct a starting model of CodPEP−CGTACG. The DNA hexamer CGTACG was constructed using QUANTA

(version 4.0, MSI, Waltham, MA). The metal binding domain of CodPEP was placed in the minor groove of the DNA close to the 5′-GT-3′ cleavage site. The bithiazole tail was placed between the T9·A4 and A10·T3 base pairs.

Structural refinements were carried out by the procedure SPEDREF (Robinson & Wang, 1992) using 992 NOESY volumes for CGTACG, 194 NOESY volumes for CodPEP, and 193 intermolecular NOEs between CodPEP and CGTACG. Sixty of the intermolecular NOEs could be measured with confidence in the NOESY spectra in D_2O and H_2O. The remaining intermolecular NOE cross peaks were less certain due to either overlap or weak cross peaks. The starting models were refined within the program X-PLOR (Brünger, 1993) in conjunction with the SPEDREF procedure. Initially, the molecule was refined with only NOE-restrained conjugate gradient minimization. The molecule then underwent a 40-step minimization routine. During the first 20 refinement cycles of this routine, the molecule was given a random set of velocities equivalent to 300 K. NOE-restrained simulated annealing was then run for 0.1 ps, the temperature coupling bath lowered by 25°, and the process repeated until the molecule had been cooled to 40 K. Each molecular dynamics cycle was carried out for a total of 10.4 ps. At this point, an additional 100 cycles of NOE-restrained conjugate gradient minimization were run. During the last 20 cycles, the molecules were refined with only NOE-restrained conjugate gradient minimization. The simulated NOE relaxation rates and NOE intensities for the refined model were calculated by the program MORASS (Post et al., 1990). Simulated 2D-NOESY spectra were produced by the program CSL (in SPEDREF package). The NMR *R*-factor is defined as *R*-factor $= \sum|N_o - N_c|/\sum N_o$, where N_o and N_c are the experimental and calculated NOE integrals, respectively.

RESULTS

Formation of PEP−DNA complexes. In order to facilitate the two-dimensional NMR analysis of PEP−DNA complexes, various DNA oligomers were treated with HO_2^-−Co(III)−CoPEP (CoPEP) or HO_2−$^-$Co(III)−CodPEP (CodPEP) and examined for the presence of a single drug binding site and a single DNA cleavage site. The self-complementary oligomer CGTACG was chosen from among these DNA oligomers for detailed structural studies. CGTACG was treated with 1 equiv of CodPEP and irradiated with UV light at 366 nm. The reaction mixture was separated by HPLC. Three DNA peaks were detected corresponding to an intact DNA strand, a DNA strand with a 4′-hydroxylated abasic site, and a free T base (Figure S1; see Supporting Information). These results confirmed that the reaction of CodPEP with CGTACG produced a single strand lesion at the pyrimidine nucleotide at the 5′-GT-3′ site. However, addition of 1 equiv of CodPEP to CGTACG did not completely cleave the DNA duplex during the 3 h incubation period.

The incomplete DNA cleavage can partly be explained from the NMR data. Inspection of the 2D NMR data of CodPEP−CGTACG revealed two sets of resonances corresponding to two DNA species in solution (DNA and DNA*) (Figures 3 and S2). In contrast, only one set of resonances was observed for CodPEP. The presence of 60 notable intermolecular NOEs between CodPEP and one of the DNA species (vide infra) indicates that a stable CodPEP−DNA

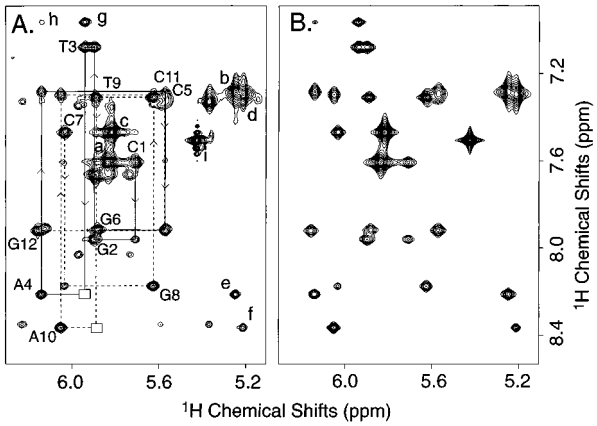

FIGURE 3: (A) Experimental and (B) simulated 2D-NOESY spectra of CodPEP−CGTACG. The dyad symmetry of the hexamer is lost. The sequential assignment pathway is illustrated (strand 1, straight lines; strand 2, dotted lines). A break in the sequential connectivity between the TpA steps is indicated with a box. The cytidine H5-H6 cross peaks are labeled (a) C1, (b) C5, (c) C7, and (d) C11. Cross peaks between C5-H5 → A4-H8 and C11-H5 → A10-H8 are labeled (e) and (f), respectively. Cross peaks between CodPEP and CGTACG are labeled (g) B-H5 → T3-H1′ and (h) B-H5 → A4-H1′. The interresidue H-H4 → H-Hβ cross peak is labeled (i). All other cross peaks in experimental spectrum A belong to the DNA* species. Since the cross peaks of the DNA* species were not used for the refinement of the CodPEP−CGTACG species, these cross peaks do not appear in simulated spectrum B.

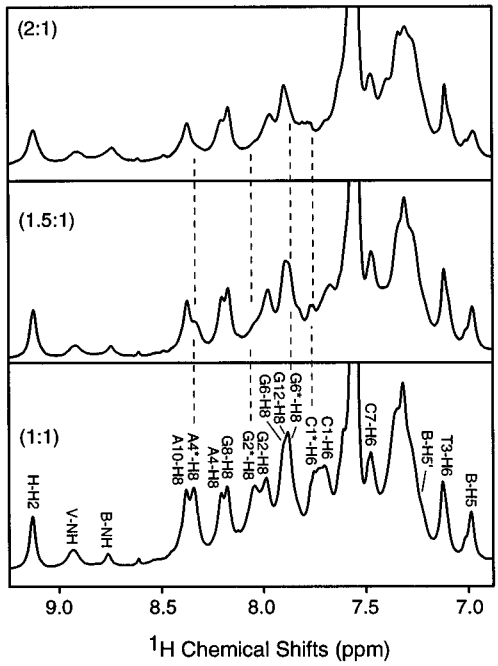

FIGURE 4: Addition of CodPEP to a 4 mM 1:1 CodPEP−CGTACG solution monitored by proton 1D NMR spectroscopy. Aromatic regions of the 1:1, 1.5:1, and 2:1 CodPEP−CGTACG complexes are shown. The resonances corresponding to the two DNA species are labeled. The dotted lines show the resonances of DNA* decreasing as excess CodPEP is added.

complex has formed. Titration of the CodPEP−CGTACG complex from 1:1 to 2:1 (Figure 4) showed a decrease in one of the DNA species (DNA*). However, the appearance of a second set of drug peaks was not observed in the 1D profile even at a ratio of 2:1 drug:DNA. The decrease in intensity of the DNA* species upon titration with CodPEP and the absence of a second set of drug peaks even at 2:1 drug:DNA may suggest that a second CodPEP−DNA complex is present in solution and is in fast equilibrium

Table 1: Chemical Shifts (ppm) for the Protons in the CodPEP−d(CGTACG)$_2$ Complex

	Proton Chemical Shifts (ppm) of d(CGTACG)$_2$[a]									
DNA	H6/H8	H2/H5/Me	H1′	H2′	H2″	H3′	H4′	H5′/H5″	imino	amino
strand 1										
C1	7.61	5.84	5.71	2.02	2.39	4.68	4.04	3.69/3.69		8.11/7.11
G2	7.96		5.90	2.58	2.66	4.95	4.32	4.09/3.99	12.83	nd
T3	7.08	1.29	5.94	2.17	2.46	4.90	4.17	4.21/3.99	13.66	
A4	8.21	7.35	6.14	2.63	2.93	4.85	4.44	4.21/4.11		nd
C5	7.28	5.25	5.59	2.28	2.04	4.91	4.02	4.22/4.11		8.55/6.95
G6	7.92		5.88	2.15	2.63	4.49	3.84	3.91/3.87	13.40	nd
strand 2										
C7	7.47	5.82	6.03	2.56	1.80	4.74	4.07	3.65/3.63		8.83/7.38
G8	8.18		5.63	2.46	2.88	5.02	4.53	4.18/4.10	13.19	9.17/7.10
T9	7.31	1.61	5.89	2.25	1.94	4.88	3.33	4.10/3.82	13.57	
A10	8.37	7.53	6.05	2.69	2.76	4.87	4.60	4.17/4.11		nd
C11	7.29	5.21	5.57	2.27	1.92	4.79	4.18	4.16/4.11		8.26/6.77
G12	7.92		6.15	2.34	2.62	4.66	4.19	4.05/4.05	13.10	nd

	Proton Chemical Shifts (ppm) of Bound CodPEP[a,b]									
CodPEP	ppm	CodPEP	ppm	CodPEP	ppm	CodPEP	ppm	CodPEP	ppm
A-H$_\alpha$	3.36	P-H$_{\alpha'}$	3.72	V-H$_\alpha$	1.26	B-H5	6.97	S-H$_\delta$	4.47
A-H$_\beta$	3.49	P-NH$_{2a}$	6.65	V-H$_\beta$	3.47	B-H5′	7.13	S-CH$_3$	1.73
A-H$_{\beta'}$	2.63	P-NH$_{2b}$	10.51	V-H$_\gamma$	3.80	B-H$_\alpha$	2.26	S-H$_\alpha$	3.34
A-NH	5.96	P-C(O)NH$_{2a}$	6.73	V-CH$_{3\gamma}$	0.97	B-H$_{\alpha'}$	2.48	S-H$_{\alpha'}$	3.27
A-NH$_{2a}$	3.88	P-C(O)NH$_{2b}$	7.73	V-NH	8.92	B-H$_\beta$	2.96	S-H$_\beta$	1.95
A-NH$_{2b}$	4.22	H-H2	9.12	V-OH	6.73	B-H$_{\beta'}$	3.90	S-H$_{\beta'}$	1.99
A-C(O)NH$_{2a}$	6.73	H-H4	7.51	T-CH$_3$	1.26	B-NH	8.74	S-H$_\gamma$	2.92
A-C(O)NH$_{2b}$	7.53	H-H$_\alpha$	4.86	T-H$_\beta$	4.55	S-Ho	7.54	S-H$_{\gamma'}$	3.11
P-CH$_3$	2.73	H-H$_\beta$	5.43	T-H$_\alpha$	4.60	S-Hm	7.54	S-NH	8.46
P-H$_\beta$	5.15	H-NH	13.32	T-NH	9.72	S-Hp	7.54	−OOH	8.39
P-H$_\alpha$	2.82	V-CH$_{3\alpha}$	0.69						

[a] Exchangeable and nonexchangeable proton data at 2 °C. [b] The protons are labeled according to the fragments shown in Figure 1: A, P, H, V, T, B, and S. CodPEP does not contain the sugars G and M.

between free and complexed drug−DNA* (Figure S3). This fast equilibrium between free and bound forms has been observed for a Zn−BLM−DNA complex (Manderville et al., 1994, 1995). In that complex, ZnBLM was bound to DNA in a nonintercalative fashion. Interestingly, the drug resonances in the Zn−BLM−DNA complex had broadened significantly, and very few NOEs were observed between Zn−BLM and the DNA. Whether CodPEP is binding to the DNA* species in a nonintercalative manner cannot be determined from the present data. On the other hand, the fact that the DNA* species is not involved in a stable CodPEP−DNA complex, and therefore probably not undergoing DNA strand scission, can account for the lowered percentage of DNA cleavage observed for this hexamer.

NMR Analysis of CodPEP−CGTACG. The stable CodPEP-CGTACG complex was fully characterized by 2D NMR and molecular modeling. The resonance assignments of CodPEP−CGTACG proceeded as described previously (Akkerman et al., 1988, 1990; Hare et al., 1983) and are listed in Table 1. In the absence of CodPEP, the self-complementary hexamer CGTACG gives rise to one set of resonances (e.g., C1-H6 and C7-H6 resonate at 7.66 ppm) (Figure 5A). Addition of CodPEP to CGTACG causes disruption of the dyad symmetry of the duplex, giving rise to two sets of resonances for these protons (e.g., C1-H6 at 7.61 ppm and C7-H6 at 7.47 ppm) (Figure 5B). Addition of CodPEP to CGTACG also caused broadening and shifting of many DNA and drug resonances (Figures 5 and 6). Selected proton resonances in the metal binding domain of CodPEP exhibited downfield shifts, while those in the DNA binding domain of CodPEP exhibited upfield shifts (Figure 6). In the metal binding domain, the pyrimidine propionamide P-CH$_3$ proton resonance shifted downfield from 2.49 to 2.73 ppm upon complexation. One of the P-NH$_2$ proton resonances shifted downfield ∼2.9 ppm to 10.51 ppm, while the other P-NH$_2$ proton resonance shifted upfield ∼1 ppm to 6.65 ppm upon complexation. Similarly, the imidazole H-H2 proton resonance of the β-hydrohistidine group shifted downfield from 8.74 ppm (free CodPEP) to 9.12 ppm (bound CodPEP). In addition, the imidazole H-NH proton resonance, which is not observed in the free drug probably due to fast exchange, is observed at 13.32 ppm in the CodPEP−DNA complex. In the DNA binding domain of CodPEP, the bithiazole B-H5 proton resonance shifted upfield from 8.06 ppm (free drug) to 6.97 ppm (bound drug), and the B-H5′ proton resonance shifted upfield from 7.88 ppm (free) to 7.13 ppm (bound).

Similar patterns were observed for the DNA (Figure 6). Certain proton resonances exhibited downfield shifts and others exhibited upfield shifts. The imino proton resonance of G8 shifted downfield by 0.31 ppm to 13.19 ppm, and one of the amino resonances of G8 resonates further downfield (at 9.17 ppm) from other G amino proton resonances (∼8.5 ppm). Selected resonances of T9, A4, and T3 exhibited upfield, rather than downfield, shifts. The H2′/2″ resonances of T9 shifted upfield from 2.19 and 2.49 ppm, respectively (free DNA), to 1.94 and 2.25 ppm (complexed DNA). The H4′ proton resonance of T9 exhibited a significantly upfield shift from 4.23 ppm (free DNA) to 3.33 ppm (complexed DNA), and the H5′ proton shifted 0.31 ppm, appearing at 3.82 ppm. These important changes in chemical shift are summarized in Figure 6.

The chemical shift changes can be explained using the NOESY data and the refined model. Tables 2 and 3 list the intermolecular NOEs between CGTACG and CodPEP. There are 35 NOE cross peaks between the metal binding

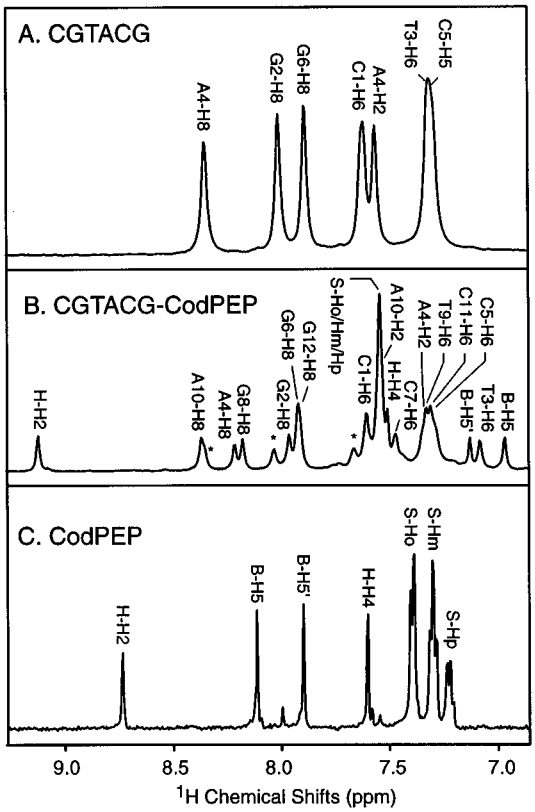

FIGURE 5: One-dimensional ^{1}H spectra of the aromatic region of (A) CGTACG, (B) the CodPEP−CGTACG complex, and (C) CodPEP. The protons are labeled according to Table 1. DNA and CodPEP resonances shift upon complexation. The largest shifts are observed for the H-H2, B-H5, B-H5′, and T3-H6 proton resonances. The phenyl proton resonances S-Ho/Hm/Hp coalesce into one peak upon complex formation. Asterisks indicate the presence of a minor species.

domain of CodPEP and the DNA hexamer. Of particular interest are the NOEs between the pyrimidinyl P-CH_3 protons and the sugar protons of G8 and T9 and between the 4-amino protons P-$NH_{2a,b}$ and the sugar protons of G8. Moderate to strong NOEs between P-CH_3 and the G8-H1′/H4′ protons and the T9-H4′/H5′/H5″ protons suggest that the drug's metal binding domain is located near G8 and T9 in the minor groove of the DNA. The presence of moderate NOEs between the 4-amino protons P-$NH_{2a,b}$ and the 2-amino protons of G8 (Figure 7) position the pyrimidinyl group of CodPEP closer to the base of G8. In agreement with this reasoning is the absence of NOEs between P-CH_3 or P-$NH_{2a,b}$ and the G8-H8 proton or the T9-H6/CH_3 protons, which are located in the major groove.

Additional NOEs between the metal binding domain of CodPEP and the DNA defined the orientation of the axial ligands of CodPEP (A-NH_2 and HO_2^-). NOEs between the pyrimidinyl protons P-Hα/Hβ, the β-aminoalanine protons A-Hβ/Hβ' of CodPEP, and the H3′, H4′, H5′, and H5″ protons of G6 place these groups and, therefore, the axial ligand A-NH_2 in the direction of the G6·C7 base pair. NOEs between the hydrogen peroxide proton and the H5′ proton of T9 placed the HO_2^- axial ligand in the direction of the T9·A4 base pair.

The position of the bithiazole DNA binding tail relative to the DNA hexamer was defined by 25 NOEs between the bithiazole S group of CodPEP and the DNA. The bithiazole B-H5 proton has many NOE cross peaks with the protons of T3 and A4, whereas the B-H5′ proton has NOE cross peaks to the protons of T9. The S-Hα/Hα', S-Hβ/Hβ', and S-Hγ/Hγ' protons of the S group of CodPEP display NOEs to T3-CH_3 while the S-Ho, S-Hm, and S-Hp protons display NOEs to T9-CH_3. These NOE cross peak patterns indicate that the DNA binding tail is close to the T9·A4 and A10·T3 base pairs. There is a break in the sequential connectivity between T3-A4 and T9-A10 (Figure 3). These findings resemble the NMR profiles observed for other BLM−DNA complexes (Mao et al., 1996; Wu et al., 1994, 1996a,b) and are indicative that *the bithiazole tail is intercalated between the T9·A4 and A10·T3 base pairs.*

Three-Dimensional Structure of CodPEP−CGTACG. On the basis of the above information, a CodPEP−CGTACG model was constructed. CodPEP was oriented with the metal binding domain in the minor groove of the DNA close to G8 and T9. The bithiazole tail, which is in a *trans* configuration (Caceres-Cortes et al., 1997), was intercalated between the T9·A4 and A10·T3 base pairs. It was oriented such that the B-H5′ proton of the first thiazole ring pointed in the direction of T9 and A10 and the B-H5 proton of the second thiazole ring pointed toward T3 and A4. The model was refined as described previously under Materials and Methods. The refined structure is shown in Figure 8. The NMR *R*-factor is 28.5%, and the agreement between the experimental and calculated NOE data can partly be seen in Figure 3.

In the refined structure, the pyrimidinyl ring is paired with the purine ring of G8 so that two hydrogen bonds [between the G8-NH_2 and the P-N3 of CodPEP (2.0 Å) and between G8-N3 and P-NH_{2b} of CodPEP (1.7 Å)] are formed (Figure 9). Hydrogen bonding of these protons is consistent with the significant downfield shifts observed for one of the 4-amino P-NH_2 proton resonances of CodPEP and one of the G8 amino proton resonances of the DNA. *These hydrogen bonds provide the sequence selectivity of the 5′-G-pyrimidine-3′ for this drug.*

The propionamide and β-aminoalanine groups are close to G6, allowing the formation of hydrogen bonds between the propionamide P-C(O)NH_2 proton and the sugar O4′ oxygen of G6 (2.3 Å), between the P-C(O)NH_2 oxygen and the 3′ OH proton of G6 (1.7 Å), and between the β-aminoalanine A-C(O)NH_2 proton and the 3′ oxygen of G6 (1.7 Å). This orientation of the metal binding domain brings the bound HO_2^- group close to the H4′ proton of T9 (2.9 Å) (Figure 8). This explains the cleavage activity for CGTACG at the 5′-GT-3′ site due to the abstraction of the T-H4′ hydrogen. The large upfield chemical shift observed for the T9-H4′ proton and the NOE observed between the T9-H5′ proton and the HO_2^- proton also support such an arrangement. Unequivocal observation of an NOE cross peak between the H4′ proton of T9 and the HO_2^- proton could not be made due to spectral overlap.

The orientation of the metal binding domain placed the V-T fragment in the minor groove of the DNA close to the T9 and A10 nucleotides. A hydrogen bond between the V-OH proton and the A10-O5′ oxygen (1.6 Å) helps anchor this group in the minor groove. This orientation allows the bithiazole tail to intercalate between T9·A4 and A10·T3 base pairs with partial stacking of the first thiazole ring between the bases of T9 and A10 and complete stacking of the second thiazole ring between the bases of T3 and A4 (Figure 10). This intercalation mode is in agreement with the larger shift

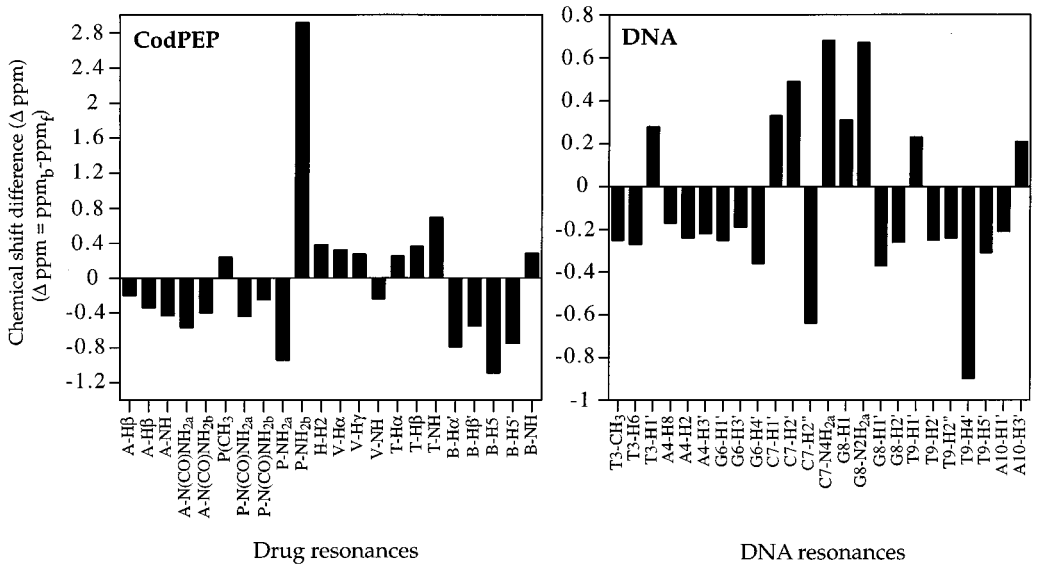

FIGURE 6: Graphs depicting chemical shift differences for CodPEP and CGTACG between the free and complex forms. Chemical shift differences greater than ±2 ppm are shown. Chemical shift differences (Δ ppm) were determined by subtracting the chemical shift of the bound complex (ppm_b) from the chemical shift chemical shift of the free drug or DNA (ppm_f). The largest chemical shift differences are observed for the pyrimidine P-NH_{2b} proton and for the T9-H4′ proton.

Table 2: Experimental (N_o) and Calculated (N_c) Interresidue NOE Cross Peak Intensities between Nonexchangeable Protons for CodPEP−CGTACG

NOEs between CGTACG and the Metal Binding Domain of CodPEP							
NOEs	N_o	N_c	distance[a]	NOEs	N_o	N_c	distance[a]
P-CH_3 → G8-H1′	240	295	2.7	V-$CH_{3\gamma}$ → T9-H5′	112	196	4.1
P-CH_3 → G8-H2′	198	146	4.6	V-$CH_{3\gamma}$ → T9-H5″	140	204	3.7
P-CH_3 → G8-H2″	193	208	3.7	P-Hα → G6-H4′	165	147	4.1
P-CH_3 → G8-H3′	154	173	4.3	P-Hα′ → G6-H4′	211	167	4.6
P-CH_3 → G8-H4′	233	249	2.4	P-Hβ → G6-H4′	151	146	4.8
P-CH_3 → G8-H5′	100	140	4.3	A-Hβ → G6-H4′	515	448	2.5
P-CH_3 → G8-H5″	148	162	4.4	A-Hβ → G6-H5′	124	146	4.5
P-CH_3 → T9-H4′	204	230	3.3	A-Hβ → G6-H5″	115	136	4.6
P-CH_3 → T9-H5′	233	272	2.8	A-Hβ′ → G6-H4′	222	251	3.5
P-CH_3 → T9-H5″	104	160	4.3	A-Hα → G6-H4′	206	257	3.4
V-$CH_{3\gamma}$ → T9-H4′	193	283	2.7				
NOEs between CGTACG and the DNA Binding Domain of CodPEP							
NOEs	N_o	N_c	distance[a]	NOEs	N_o	N_c	distance[a]
B-H5 → T3-H6	132	244	4.1	B-H5 → A4-H5′	232	227	3.6
B-H5 → T3-CH_3	128	125	5.3	B-H5 → A4-H5″	198	209	3.7
B-H5 → T3-H1′	204	258	3.2	B-H5 → T9-H6	165	156	4.8
B-H5 → T3-H2′	251	231	3.3	B-H5 → T9-CH_3	192	177	4.2
B-H5 → T3-H2″	242	335	2.6	S-Ho-p → T9-CH_3	56	21	6.5
B-H5 → T3-H3′	152	145	4.5	S-Hα → T3-CH_3	196	147	4.7
B-H5 → A4-H8	201	226	3.6	S-Hα′ → T3-CH_3	216	190	3.4
B-H5 → A4-H2	119	136	4.8	S-Hβ → T3-CH_3	175	228	3.1
B-H5 → A4-H1′	194	181	4.3	S-Hβ′ → T3-CH_3	156	191	4.3
B-H5 → A4-H2′	126	123	4.9	S-Hγ → T3-CH_3	84	80	5.9
B-H5 → A4-H2″	141	137	4.6	S-Hγ′ → T3-CH_3	112	118	5.1
B-H5 → A4-H4′	200	196	4.1				

[a] Distances in angstroms (Å) were derived from the refined model of CodPEP−CGTACG. N_o, experimental NOE intensities; N_c, calculated NOE intensities.

of the B-H5 proton resonance (−1.09 ppm) relative to the B-H5′ proton resonance shift (−0.75 ppm). Concomitantly, the base protons of T3-A4 have larger upfield shifts and T9-A10 protons have smaller upfield shifts. Some buckling of the T9·A4 and A10·T3 base pairs, a feature not unlike that found in anthracycline−DNA complexes (Wang, 1992), is found.

Intercalation of the bithiazole moiety places the S group in the major groove where the phenyl group has some freedom to rotate. This flexibility of the S group is consistent with the shorter T_1 relaxation times for the protons of the S group and with the finding that the phenyl S-Ho/Hm/Hp resonances have now coalesced into one peak. In contrast, these phenyl protons are resolved in the free CoPEP and CodPEP molecules (Caceres-Cortes et al., 1997).

Comparison of the structure of CodPEP in its free and bound state reveals that the structure of the metal binding domain has not changed significantly upon complexation (Figure S4). The largest structural differences are observed for the threonine fragment and the bithiazole moiety and S group of the DNA binding domain. Rotations around the amide and Cα−Cβ bonds of the T, B, and S moieties allow

Table 3: Intermolecular NOE Cross Peak Intensities between Exchangeable Protons of CodPEP−CGTACG

NOEs	N_r[a]	distance[b]	NOEs	N_r[a]	distance[b]
P-NH_{2a} → G8-NH_{2a}	w	3.9	P-NH_{2b} → T9-H1′	w	3.8
P-NH_{2a} → G8-H1′	s	1.9	P-C(O)NH_{2a} → G8-NH_{2a}	m	3.4
P-NH_{2a} → G8-H4′	s	2.4	P-C(O)NH_{2a} → G8-NH_{2b}	m	3.2
P-NH_{2a} → G8-H5′	w	4.0	HO_2^- → T9-H1′	w	3.2
P-NH_{2b} → G8-NH_{2a}	m	2.3	HO_2^- → T9-H4′	ov	2.9
P-NH_{2b} → G8-NH_{2b}	w	3.7	HO_2^- → T9-H5′	vw	5.1
P-NH_{2b} → G8-H1′	s	2.4	B-H5′ → T9-H_3	w	4.7
P-NH_{2b} → G8-H4′	w	4.0	S-NH → T3-CH_3	w	4.0
P-NH_{2b} → G8-H5′	vw	5.1			

[a] N_r, relative intensities based on visual inspection of the NOESY cross peaks. [b] Distances in angstroms (Å) were derived from the refined model for CodPEP−CGTACG. s, strong; m, medium; w, weak; vw, very weak; ov, overlap.

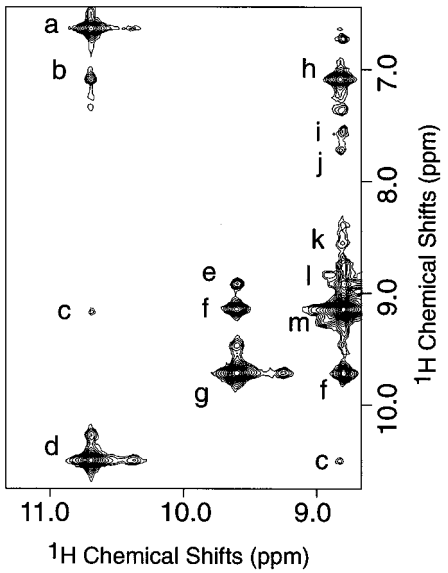

FIGURE 7: Portions of the exchangeable proton 2D-NOESY spectrum of CodPEP−CGTACG. Selected cross peaks are labeled (a) P-NH_{2a} → P-NH_{2b}, (b) P-NH_{2b} → G8-NH_{2a}, (c) P-NH_{2b} → G8-NH_{2b}, (d) diagonal P-NH_{2b}, (e) T-NH → V-NH, (f) T-NH → H-H2, (g) diagonal T-NH, (h) G-NH_{2a} → G-NH_{2b}, (i) H-H2 → H-H4, (j) G8-NH_{2b} → P-C(O)NH_{2b}, (k) G8-NH_{2b} → C5-NH_{2b} (l) H-H2 → V-NH, and (m) diagonal G8-NH_{2b}/H-H2.

the DNA binding tail to flip between a folded conformation (in its free form) and an extended conformation (when bound to DNA). This gating motion of the DNA binding domain facilitates intercalation of the bithiazole moiety between DNA base pairs, thereby exposing the hydroperoxide group and allowing it to react with the DNA.

DISCUSSION

Bleomycin (BLM) and its analog pepleomycin (PEP) have been the subject of intense investigations for over 2 decades. One of the issues that remained unresolved until very recently was the nature of the axial ligands around the metal center. Previous reports had proposed that the β-aminoalanine primary amine A-NH_2 was the preferred axial ligand in cobalt−bleomycin species (Xu et al., 1994; Wu et al., 1996a). Recent studies from our laboratory of two cobalt−pepleomycin species, HO_2^-−Co(III)−PEP (CoPEP) and deglycosylated HO_2^-−Co(III)−PEP (CodPEP) (Caceres-Cortes et al., 1997), revealed that the preferred axial ligand in CoPEP is not A-NH_2 but the mannose carbamoyl moiety, M-NH_2. It is only in the absence of the disaccharide moiety, as in CodPEP, that the A-NH_2 group comes to occupy the axial position. In light of our recent findings, and the previous reports that Fe−BLM and deglycosylated Fe−BLM cleaved the oligonucleotide d($CGCT_3A_3GCG$)$_2$ at different sites (Sugiyama et al., 1986), we set out to characterize the interaction of CoPEP and deglycosylated CoPEP with DNA.

CodPEP cleaves CGTACG in the presence of UV light, producing a single strand scission at the 5′-GT-3′ site (Figure S1). CGTACG was titrated with CodPEP, and the resulting 1:1 complex was studied by ^{1}H NMR. The interaction between CodPEP and CGTACG is best described by referring to the different functional domains of the drug, i.e., the metal binding domain and the DNA binding domain. The metal binding domain resides in the minor groove of the DNA close to G8 and T9 (Figure 8), and the pyrimidine ring of the drug forms a base triplet with the G8·C5 base pair of the DNA via two hydrogen bonds (Figure 9). This triple-base formation has also been observed for a Co−BLM−d($CCAGGCCTGG$)$_2$ complex (Wu et al., 1996b). The formation of this base triplet between the pyrimidine ring of the drug and the purine ring of G8 confers the sequence selectivity of this drug for 5′-G-Pyr-3′ sites. Cleavage at 5′-A-Pyr-3′ has been observed, although to a smaller extent than at 5′-G-Pyr-3′ sites (Boger et al., 1995), likely due to a less stable base triplet. And cleavage at 5′-C-Pyr-3′ and 5′-T-Pyr-3′ is significanlty lower (less than 5%), probably due to the inability to form a stable base triplet. The preference for 5′-G-*pyrimidine*-3′ versus 5′-G-*purine*-3′ is less clear. Cleavage has been observed for pyrimidines in 5-GC-3′ and 5′-GT-3′ sites and for adenines in 5′-GA-3′ (although to a lesser extent than C and T). Interestingly, cleavage at 5′-GG-3′ sites was not observed. On the basis of our model, there are no hydrogen-bonding networks or steric factors between CodPEP and the pyrimidine at the 5′-GT-3′ cleavage site that would explain the preference for pyrimidines versus purines at this site. Other factors, such as the preference of intercalators for 5′-Pyr-X-3′ sites (X being any nucleotide) or the inherent chemistry at this position may be responsible for the C, T > A >>> G preference.

DNA cleavage is initiated by abstraction of the H4′ hydrogen of the pyrimidine in 5′-GC-3′ and 5′-GT-3′ sequences by the ·OH free radical generated from the hydroperoxide group of CodPEP through homolysis upon UV radiation. Our model places the distal oxygen of the HO_2^- group of CodPEP within 2.9 Å from the T9-H4′ proton in the minor groove, adequate for C4′ proton abstraction. The anchoring of the pyrimidine ring of CodPEP to the purine ring of G8 severely restricts the movement of the metal binding domain and, therefore, does not favor abstraction of other sugar protons of T9.

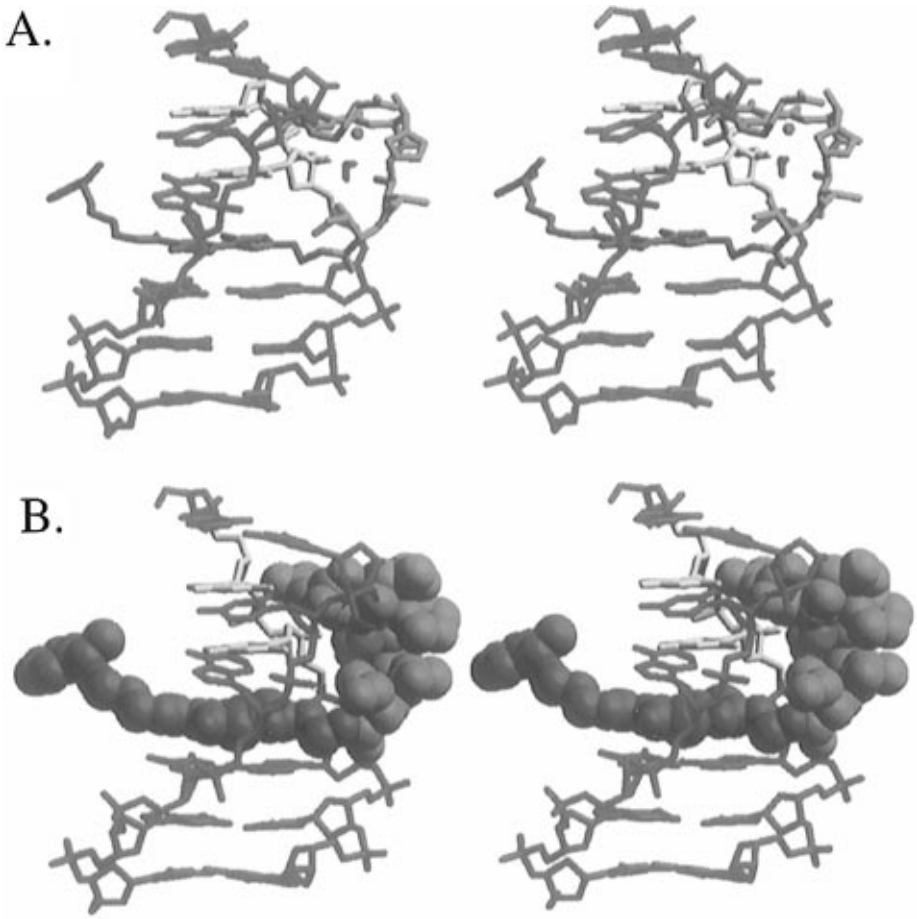

FIGURE 8: Stereo drawings of the refined CodPEP−CGTACG complex (*R*-factor 28.5%). In (B), CodPEP appears as van der Waals spheres. For clarity, the protons have been omitted except for T9-H4′, HO_2^-, B-H5 and B-H5′. DNA is drawn in blue, the G8-T9 cleavage site in yellow, and the T9-H4′ proton in light gray. The metal binding domain of CodPEP is drawn in green, the HO_2^- group in purple, and the bithiazole group in yellow. The cobalt ion is shown as an orange sphere. The metal binding domain of CodPEP binds in the minor groove of the DNA close to the G8-T9 nucleotides. The pyrimidine ring of CodPEP forms a base triplet with the G8•C5 base pair by means of hydrogen bonds. The bithiazole tail is intercalated between the TpA steps. This orientation brings the hydroperoxide group within 2.9 Å from T9-H4′, excellent for hydrogen abstraction.

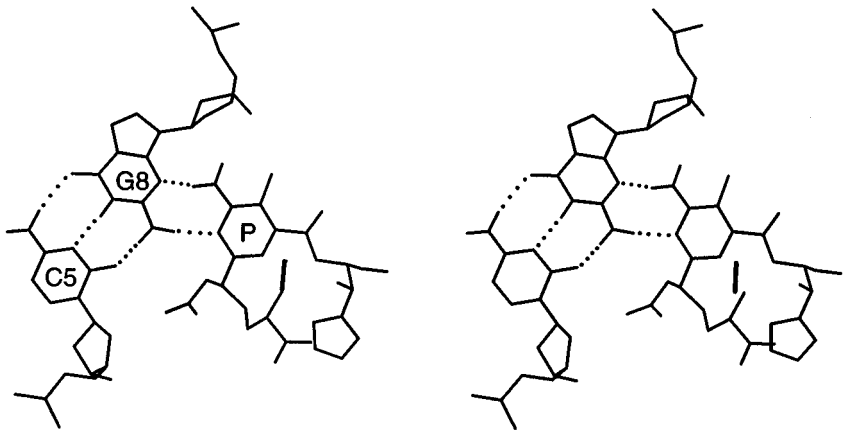

FIGURE 9: Base triplet formation between the pyrimidine of CodPEP (P) and the G8•C5 DNA base pair. Hydrogen bonds between P-N3 and G8-NH_2 and between P-NH_2 and G8-N3 are indicated with dotted lines.

Cleavage of DNA by CodPEP involves the unfolding of the compact CodPEP (Figure 11), threading of the bithiazole tail between base pairs, and finally positioning of the HO_2^- group close to the T or C found 3′ to the specific G site. The unfolding and intercalation of the bithiazole tail have also been observed for a related BLM−DNA complex (Wu et al., 1994, 1996a,b). In contrast, a Zn−BLM−DNA complex (Manderville et al., 1994, 1995) and a CoPEP−DNA complex (data not shown) place the bithiazole tail spanning along the minor groove of the DNA in a non-intercalative fashion. The observation of two different binding modes may be important in understanding the DNA cleaving activity *in vivo*. It is likely that, at the physiological concentration level of PEP/BLM, the drugs bind to DNA initially in the nonintercalative mode, which does not permit the HO_2^- group to be in direct contact with DNA. Only when PEP/BLM encounters 5′-GC or 5′-GT sequences where the drug molecule unfolds and intercalates its bithiazole

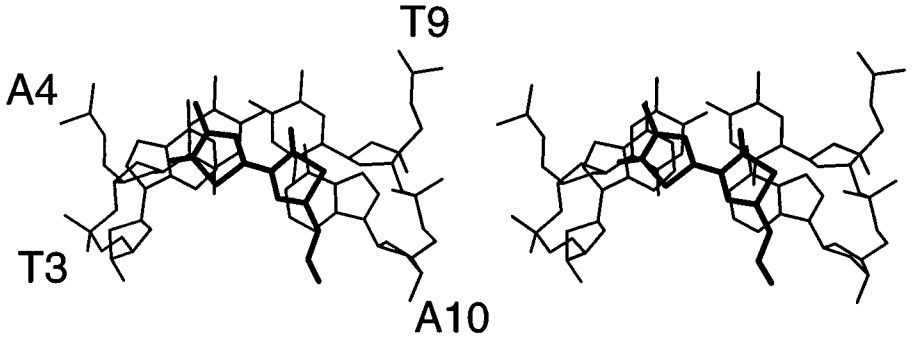

FIGURE 10: Stacking diagrams (top view) surrounding the bithiazole moiety of CodPEP. For clarity, only the two base pairs directly adjacent to the bithiazole moiety are shown. The bithiazole moiety appears as thick lines, and the nucleotides (thin lines) are labeled. The first thiazole ring is partially stacked between the T9-A10 nucleotides. The second thiazole ring is stacked between the T3-A4 nucleotides.

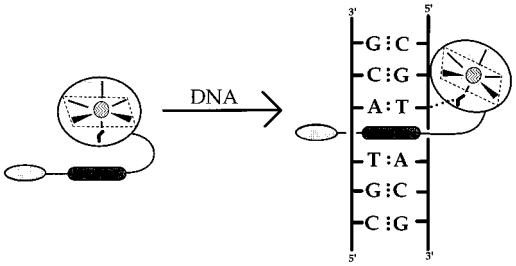

FIGURE 11: Schematic representation of the binding of CodPEP to CGTACG. CodPEP adopts a compact form in solution with the bithiazole tail folded toward the metal binding domain. Upon binding to CGTACG, the metal binding domain recognizes and binds to the minor groove at the GpT site. The bithiazole tail intercalates between the TpA sites, exposing the hydrogen peroxide group to initiate strand scission at the T nucleotide.

group, thereby creating a stable long-lived complex in which HO_2^- is in direct contact with H4′ proton, can radical H-atom abstraction take place.

While there appears to be no sequence-specific interactions between the bithiazole group of CodPEP and CGTACG, this moiety helps stabilize the drug−DNA complex by intercalating between the T9·A4 and A10·T3 base pairs (Figure 10), placing the S group in the major groove of the DNA. This is evident from the large number of NOEs between the base protons of T3-H6/CH3 and A4-H8 and the S-Hα/Hα', S-Hβ/Hβ', and S-Hγ/Hγ' protons of CodPEP. While the $-(CH_2)_3-$ chain of the S group appears to be in a fixed position in the major groove, the phenyl group seems to have some degree of flexibility. This is inferred from the observation that the proton resonances of the *ortho*, *meta*, and *para* protons of the phenyl group appear coalesced into one peak in the ^{1}H spectrum.

It has been postulated that the positively charged sulfonium group of BLM A_2 helps anchor the bithiazole moiety through electrostatic interactions between the sulfonium group and the negatively charged region of the DNA (Wu et al., 1996b). In addition, the sulfonium group is thought to have a limited range of motion once bound to the DNA, as evidenced by the nonequivalence of the sulfonium methyl proton resonances in the drug−DNA complex. In the absence of DNA, the sulfonium methyl proton resonances are equivalent, suggesting freedom of movement of this group in the free drug. The phenyl group of CodPEP displays the opposite behavior. In the free drug, the *ortho*, *meta*, and *para* protons of the phenyl group appear as three distinct signals. Once bound to DNA, these resonances coalesce into one peak, consistent with a greater degree of motion of this group in the drug−DNA complex.

In this paper, we have fully characterized the structure of deglycosylated CoPEP (CodPEP) and the DNA hexamer CGTACG. CodPEP lacks the sugars mannose and gulose in the metal binding domain. We have previously shown that the deglycosylated drug and the intact drug have different structures around the metal center. In CoPEP the sugar is participating in metal chelation and occupies an axial position, whereas in CodPEP, the β-aminoalanine primary amine is occupying the axial position. It has been shown that these differences in the metal binding domain of the intact and deglycosylated drugs affect their interactions with DNA. For example, treatment of $d(CGCT_3A_3GCG)_2$ with Fe−BLM and deglycosylated Fe−BLM results in cleavage at different sites (Sugiyama et al., 1986). Cleavage with Fe−BLM occurs predominantly at C11 while cleavage with deglycosylated Fe-BLM occurs predominantly at C3. The factors that are giving rise to these different interactions between the DNA and the intact and deglycosylated drugs are still not known.

A model of an intact Co−BLM molecule complexed with DNA has been reported very recently (Wu et al., 1996b). This model resembles the CodPEP−CGTACG model presented in this paper; i.e., the formation of a triple-base interaction between the drug's pyrimidine group and a G·C base pair is observed, and the bithiazole group is intercalated between the DNA base pairs. This BLM−DNA model however, does not contain the mannose M-NH_2 group in the axial position, as would be expected for the intact Co−BLM molecule, and therefore cannot be used to define differences between the intact drug and the deglycosylated drug. We are, therefore, currently characterizing the complex between the intact CoPEP and CGTACG. Comparisons between this complex and the deglycosylated CodPEP−CGTACG complex reported in this paper should provide useful information regarding the different interactions between these drugs and DNA.

ACKNOWLEDGMENT

We thank Dr. H. Robinson for his technical assistance and the preliminary work on CoPEP and Prof. C. Hilbers and Dr. H. Heus for their help in the use of their Unity 750 MHz spectrometer for collection of the NOESY data.

SUPPORTING INFORMATION AVAILABLE

Four figures showing the HPLC profile of CodPEP-mediated cleavage of CGTACG, the experimental 2D-NOESY spectrum of CodPEP−CGTACG with assignments

for DNA* species, a schematic representation of the binding of CodPEP to DNA*, and a comparison between the free and bound CodPEP molecules (6 pages). Ordering information is given on any current masthead page.

REFERENCES

Akkerman, M. A. J., Haasnoot, C. A. G., & Hilbers, C. W (1988) *Eur. J. Biochem. 173*, 211−225.

Akkerman, M. A. J., Neijman, E. W. J. F., Wijmenga, S. S., Hilbers, C. W., & Bermel C. W. (1990) *J. Am. Chem. Soc. 112*, 7462−7474.

Boger, D. L., Menzes, R. F., & Yang, W. (1992) *Bioorg. Med. Chem. Lett. 2*, 959−962.

Boger, D. L., Teramoto, S., & Zhou, J. (1995) *J. Am. Chem. Soc. 117*, 7344−7356.

Brünger, A. T. (1993) *X-PLOR, version 3.2*, The Howard Hughes Medical Institute and Yale University, New Haven, CT.

Burger, R. M., Berkowitz, A. E., Peisach, J., & Horwitz, S. B. (1980) *J. Biol. Chem. 255*, 11832−11838.

Burger, R. M., Peisach, J., & Horwitz, S. B. (1981) *J. Biol. Chem. 256*, 11636−11644.

Burger, R. M., Peisach, J., & Horwitz, S. B. (1982) *J. Biol. Chem. 257*, 3372−3375.

Caceres-Cortes, J., Sugiyama, H., Ikudome, K., Saito, I., & Wang, A. H.-J. (1997) *Eur. J. Biochem. 244*, 818−828.

Carter, B. J., Murty, V. S., Reddy, K. S., Wang, S.-N., & Hecht, S. M. (1990) *J. Biol. Chem. 265*, 4193−4196.

Chen, D. M., Sakai, T. T., Glikson, J. D., & Patel, D. J. (1980) *Biochem. Biophys. Res. Commun. 92*, 197−205.

Chien, M., Grollman, A. P., & Horwitz, S. B. (1977) *Biochemistry 16*, 3641−3647.

Dabrowiak, J. C., & Tsukayama, M. (1981) *J. Am. Chem. Soc. 103*, 7543−7550.

D'Andrea, A. D., & Haseltine, W. A. (1978) *Proc. Natl. Acad. Sci. U.S.A. 75*, 3608−3612.

Fisher, L. M., Kuroda, R., & Sakai, T. T. (1985) *Biochemistry 24*, 3199−3207.

Hare, D. R., Wemmer, D. E., Chow, S.-H., Droby, G., & Reid, B. R. (1983) *J. Mol. Biol. 171*, 319−336.

Hénichart, J.-P., Bernier, J. L., Heibecque, N., & Houssin, R. (1985) *Nucleic Acids Res. 13*, 6703−6717.

Hiraoki, H., Nakayama, T., Ikehara, M., & Vesigi, S. (1991) *Chem. Pharm. Bull. 39*, 2780−2786.

Hore, P. J. (1983) *J. Magn. Reson. 54*, 539−542.

Kane, S. A., Natrajan, A., & Hecht, S. M. (1994) *J. Biol. Chem. 269*, 10899−10904.

Kozarich, J. W., Worth, L., Jr., Frank, B. L., Christner, D. F., Vanderwall, D. E., & Stubbe, J. (1989) *Science 245*, 1396−1399.

Kross, J., Henner, W. D., Haseltine, W. A., Rodriguez, L., Levin, M. D., & Hecht, S. M. (1982) *Biochemistry 21*, 3711−3721.

Kuwahara, J., & Sugiura, Y. (1988) *Proc. Natl. Acad. Sci. U.S.A. 85*, 2459−2463.

Manderville, R. A., Ellena, J. F., & Hecht, S. M. (1994) *J. Am. Chem. Soc. 116*, 10851−10852.

Manderville, R. A., Ellena, J. F., & Hecht, S. M. (1995) *J. Am. Chem. Soc. 117*, 7891−7903.

Mao, Q., Fulmer, P., Li, W., DeRose, E. F., & Petering, D. H. (1996) *J. Biol. Chem. 271*, 6185−6191.

Matsuda, A., Yoshioka, O., Ebihara, K., Ekimoto, H., Yashamita, T., & Umezawa, H. (1978) in *Bleomycin: Current Status and New Developments* (Carter, S. K., Crooke, S. T., & Umezawa H., Eds.) pp 299−331, Academic Press, New York.

McGall, G. H., Rabow, L. E., & Stubbe, J. (1987) *J. Am. Chem. Soc. 109*, 2836−2837.

Mirabelli, C. K., Huang, C.-H., & Crooke, S. T. (1983) *Biochemistry 22*, 300−306.

Oka, S. (1980) *Recent Results Cancer Res. 74*, 163−171.

Post, C. B., Meadows, R. P., & Gorenstein, D. G. (1990) *J. Am. Chem. Soc. 112*, 6796−6803.

Povirk, L. F., Hogan, M., & Dattagupta, N. (1979) *Biochemistry 18*, 96−101.

Robinson, H., & Wang, A. H.-J. (1992) *Biochemistry 31*, 3524−3533.

Shipley, J. B., & Hecht, S. M. (1988) *Chem. Res. Toxicol. 1*, 25−27.

Sklenar, V., Brooks, B. R., Zon, G., & Bax, A. (1987) *J. Magn. Reson. 75*, 352−357.

States, D. J., Haberkorn, R. A., & Ruben, D. J. (1982) *J. Magn. Reson. 48*, 286−292.

Sugiyama, H., Kilkuskie, R. E., Chang, L.-H., Ma, L.-T., Hecht, S. M., van der Marel, G. A., & van Boom, J. H. (1986) *J. Am. Chem. Soc. 108*, 3852−3854.

Sugiyama, H., Kawabata, H., Fujiwara, T., Dannoue, Y., & Saito, I. (1990) *J. Am. Chem. Soc. 112*, 5252−5257.

Takahashi, K., Ekimoto, H., Aoyagi, S., Koyu, A., Kenamochi, H., Yoshioka, O., Matsuda, A., Fujii, A., & Umezawa, H. (1979) *J. Antibiot. 23*, 36−42.

Takeshita, M., Grollman, A. P., Ohtsubo, E., & Ohtsubo, H. (1978) *Proc. Natl. Acad. Sci. U.S.A. 75*, 5983−5987.

Takita, T., Murakaoka, Y., Nakatani, T., Fujii, A., Iitaka, Y., & Umezawa, H. (1978) *J. Antibiot. 31*, 1073−1077.

Wang, A. H.-J. (1992) *Curr. Opin. Biol. 2*, 361−368.

Wu, J. C., Kozarich, J. W., & Stubbe, J. (1985) *Biochemistry 24*, 7562−7568.

Wu, W., Vanderwall, D. E., Stubbe, J., Kozarich, J. W., & Turner, C. J. (1994) *J. Am. Chem. Soc. 116*, 10843−10844.

Wu, W., Vanderwall, D. E., Lui, S. M., Tang, X.-J., Turner, C. J., Kozarich, J. W., & Stubbe, J. (1996a) *J. Am. Chem. Soc. 118*, 1268−1280.

Wu, W., Vanderwall, D. E., Turner, C. J., Kozarich, J. W., & Stubbe, J. (1996b) *J. Am. Chem. Soc. 118*, 1281−1294.

Xu, R. X., Antholine, W. E., & Petering, D. H. (1992a) *J. Biol. Chem. 267*, 944−949.

Xu, R. X., Antholine, W. E., & Petering, D. H. (1992b) *J. Biol. Chem. 267*, 950−955.

Xu, R. X., Nettesheim, D., Otvos, J. D., & Petering, D. H. (1994) *Biochemistry 33*, 907−916.

BI9708951